Experimental charge densities of highly deformed halogenated fullerenes
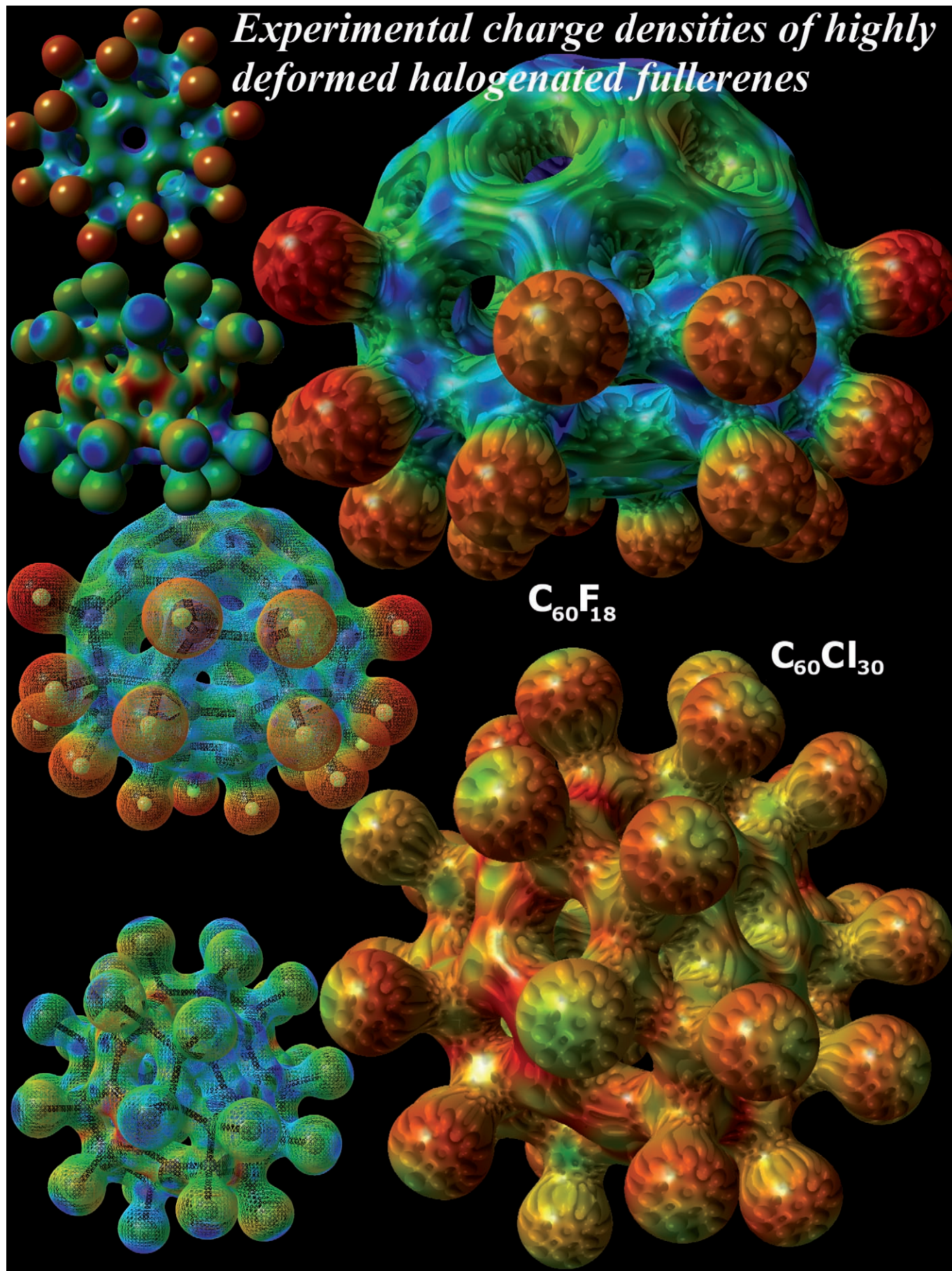
$C_{60}F_{18}$

$C_{60}Cl_{30}$

Bond Orders and Atomic Properties of the Highly Deformed Halogenated Fullerenes $C_{60}F_{18}$ and $C_{60}Cl_{30}$ Derived from their Charge Densities

Christian B. Hübschle,[a] Stephan Scheins,[a] Manuela Weber,[a] Peter Luger,*[a] Armin Wagner,[b] Tibor Koritsánszky,[c] Sergey I. Troyanov,[d] Olga V. Boltalina,[e] and Il'ya V. Goldt[d]

Abstract: The experimental charge densities of the halogenated C_{60} fullerenes $C_{60}F_{18}$ and $C_{60}Cl_{30}$ were determined from high-resolution X-ray data sets measured with conventional $Mo_{K\alpha}$ radiation at 20 K for $C_{60}Cl_{30}$ and with synchrotron radiation at 92 K for the fluorine compound. Bond topological and atomic properties were analyzed by using Bader's AIM theory. For the different C—C bonds, which vary in lengths between 1.35 and 1.70 Å bond orders n between $n=2$ and significantly below $n=1$ were calculated from the bond topological properties at the bond critical points (BCP's). The low bond orders are seen for 5/6 bonds with each contributing carbon carrying a halogen atom. By integration over Bader's zero flux basins in the electron density gradient vector field atomic properties were also obtained. In contrast to free C_{60}, in which all carbon atoms have a uniform volume of 11 Å^3 and zero charge, atomic volumes vary roughly between 5 and 10 Å^3 in the halogenated compounds. Almost zero atomic charges are also found in the Cl derivative but a charge separation up to ± 0.8 e exists between C and F in $C_{60}F_{18}$ due to the higher fluorine electronegativity, which is also seen in the electrostatic potential for which the electronegativity difference between carbon and fluorine, and the addition to one hemisphere of the fullerene cage leads to a strong potential gradient along the $C_{60}F_{18}$ molecule. From the summation over all atomic volumes it follows that the halogen addition does not only lead to a dramatic distortion of the C_{60} cage but also to a significant shrinkage of its volume.

Keywords: bond order · charge density · fullerenes · halogens · topological analysis

[a] Dipl.Chem. C. B. Hübschle, Dipl.Chem. S. Scheins, M. Weber, Prof. P. Luger
Institut für Chemie und Biochemie/Kristallographie
Freie Universität Berlin, Fabeckstr. 36a
14195 Berlin (Germany)
Fax: (+49)30-8385-3464
E-mail: luger@chemie.fu-berlin.de

[b] Dr. A. Wagner
Paul Scherrer Institut, Swiss Light Source
WSLA/220, CH-5232 Villigen PSI (Switzerland)

[c] Prof. T. Koritsánszky
Department of Chemistry
Middle Tennessee State University, P.O. Box 68
Murfreesboro, TN 37132 (USA)

[d] Prof. S. I. Troyanov, Dr. I. V. Goldt
Department of Chemistry, Moscow State University
119992 Moscow, Leninskie Gory (Russia)

[e] Prof. O. V. Boltalina
Department of Chemistry, Colorado State University
Fort Collins, Colorado 80523 (USA)

Supporting information for this article is available on the WWW under http://www.chemeurj.org/ or from the author.

Introduction

Thanks to the recent technical advances in X-ray diffraction, experimental electron density investigations on larger molecules can be performed with moderate effort, provided that properly diffracting crystals are available. Hence fullerenes with generally 60 or more atoms could in principle be studied; however, their investigation is complicated on one hand by the generally poor quality of fullerene crystals and on the other hand by the generally high mobility of these molecules in the crystal lattice. That is why only few electron density studies on highly substituted fullerenes are reported, while no such study is known for a free fullerene.[1,2]

For free C_{60}, the few chemically independent atomic and bond topological properties that can be obtained by application of Bader's quantum theory of atoms in molecules (QTAIM)[3] have been derived from theoretical calculations. Due to the high I_h molecular symmetry of the C_{60} cage, all 60 carbon atoms are chemically equivalent and only two different bonds, the 5/6 and the 6/6 bond exist, so that these

Table 1. Bond topological and atomic properties of free C_{60} (from HF/6–311G** optimization).

	5/6 bond	6/6 bond
length [Å]	1.448	1.371
$\rho(\mathbf{r}_{BCP})$ [e Å^{-3}]	1.97	2.23
$\nabla^2\rho(\mathbf{r}_{BCP})$ [e Å^{-5}]	−20.48	−25.13
ε	0.16	0.29
n	1.38	1.83
Atomic properties		
C	$V = 11.0$ Å^3	$q = 0.00$ e

atomic and bond topological properties can easily be summarized in a short table (Table 1).

The geometric and bonding situation of the C_{60} cage changes drastically if highly halogenated fullerenes, which were recently reported, are considered. Depending on the addition of specific number of fluorine, chlorine, or bromine atoms, the carbon cage can get heavily deformed.[4–7] The deformation is caused by a significant change in the C−C bond lengths, which are found in a wide range from roughly 1.35 to 1.70 Å. These dramatic changes relative to the highly symmetric free C_{60} cage should have severe influences on the electronic structure, atomic, and bond topological properties, which are subject of this study. Here we report on the experimental electron density $\rho(\mathbf{r})$ of $C_{60}F_{18}$,[5] for which the molecular structure is known to be distorted towards a "turtle" hemispherical shape (see Figure 1), and on a corresponding study on D_{3d}-$C_{60}Cl_{30}$[7] (a second isomer of $C_{60}Cl_{30}$ exists possessing the C_2-molecular symmetry), in which the distortion led to a "drum-like" conformation of the C_{60} cage (Figure 2). The focus of this study is directed to the bond orders of the different C−C bonds, and the atomic properties of the carbon atoms, which are distinguishable in contrast to free C_{60}.
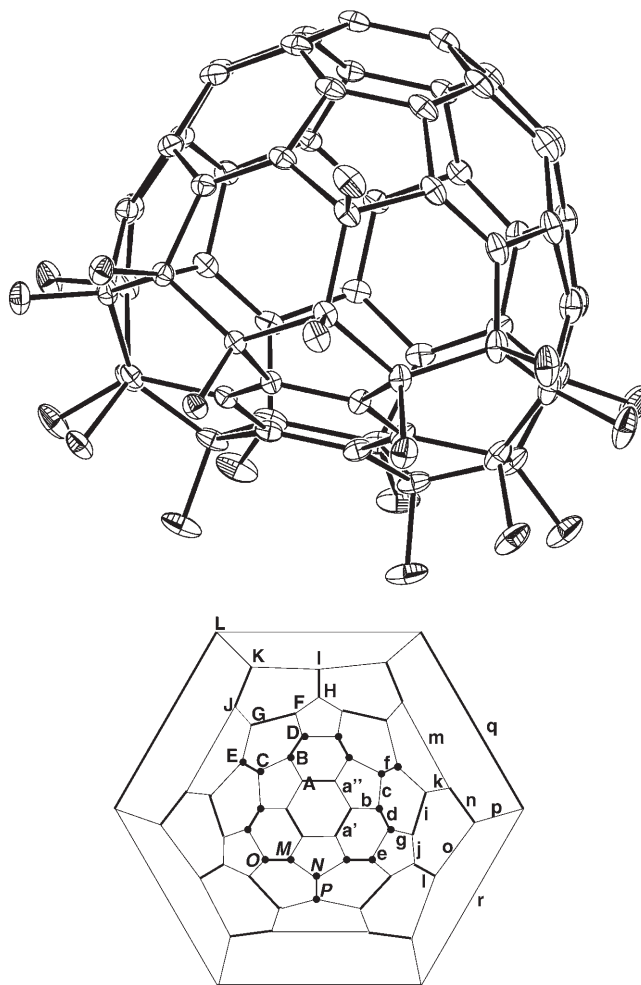

Figure 1. Top: ORTEP[34] representation of the molecular structure of $C_{60}F_{18}$ at 92 K in the crystal. Displacement ellipsoids are drawn at a 50% probability. Bottom: Schlegel diagram with bond (small letters) and atom types (capital letters).

Results and Discussion

The molecular structures as present in the crystal are displayed in Figures 1 and 2 together with the corresponding Schlegel diagrams illustrating the chosen atomic numbering scheme, and the different types of atoms and bonds that are discussed below. Quantitative interpretation of the charge density distribution was made in terms of Bader's AIM theory.[3]

Bond topological analysis: According to Bader's definition, bond critical points $\mathbf{r}_{BCP}$, which satisfy the conditions that $\nabla\rho(\mathbf{r})$ vanishes at $\mathbf{r}_{BCP}$, were located for all covalent bonds. Bond topological properties at the $\mathbf{r}_{BCP}$'s based on the multipole models and the theoretical calculations are compared.

As already mentioned, the high deformation of the C_{60} cages is result of significant changes in the C−C bond lengths. While in free C_{60} only two types of bonds exist ($r_{5/6} = 1.448$ Å, $r_{6/6} = 1.371$ Å), a large variety of bonds with different lengths are observed in halogen-substituted cages,

with the longest ones reaching rather extreme C−C bond lengths close to 1.7 Å. In Figures 3 (for $C_{60}Cl_{30}$) and 4 (for $C_{60}F_{18}$) the electron density values, $\rho(\mathbf{r}_{BCP})$, from experiment and the theoretical calculations are plotted versus the C−C bond lengths, confirming in all cases an approximate linear relation.

For $C_{60}Cl_{30}$ two parallel least-squares lines rather close together are seen for the two theoretical calculations. On an average, the HF $\rho(\mathbf{r}_{BCP})$ values are 0.05 e Å^{-3} higher than the corresponding DFT results. The experimental line is in between, so that a proper agreement between theory and experiment is found. For the fluorinated fullerene the theoretical least-squares lines are slightly further apart, by ≈ 0.1 e Å^{-3}, while the experimental spread is rather large, possibly due to the limited crystal quality discussed below in the Experimental Section.

We note that in an earlier study on a highly substituted ethoxycarbonyl-C_{60}-fullerene[1] (with a less distorted C_{60} cage) similar findings for the experimental and theoretical $\rho(\mathbf{r}_{BCP})$ versus bond length relation were derived. The C−C
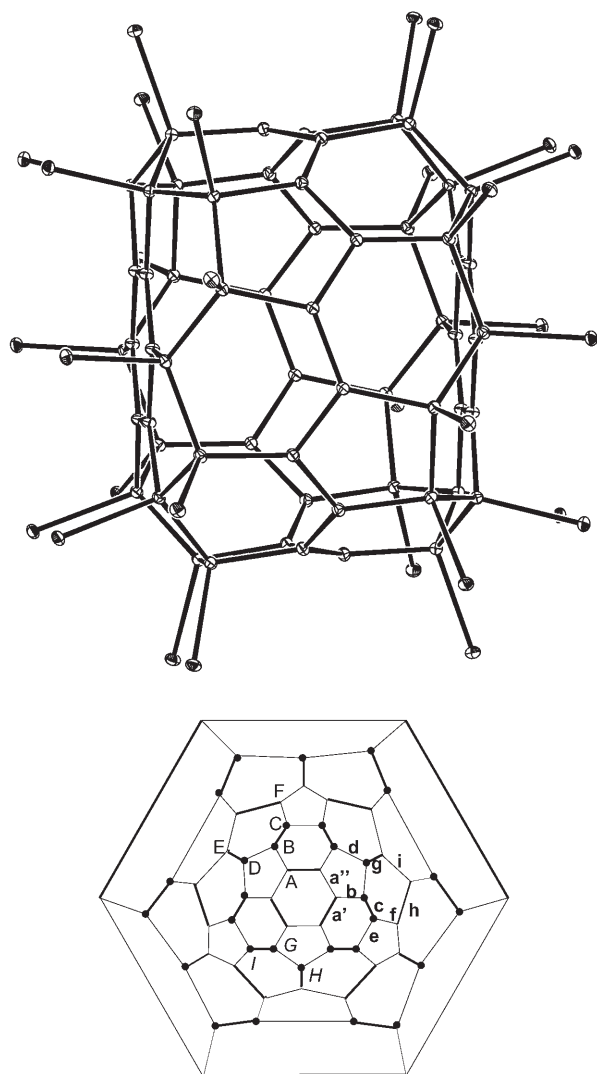
Figure 2. Top: ORTEP[34] representation of the molecular structure of $C_{60}Cl_{30}$ at 20 K in the crystal. Displacement ellipsoids are drawn at a 50% probability. Bottom: Schlegel diagram with bond (small letters) and atom types (capital letters).

bond-length range was smaller (1.40 to 1.60 Å) in that compound.

Once the topological descriptors at the bond critical points are available, topological bond orders can be calculated from the electron density values $\rho(\mathbf{r}_{BCP})$ and the principal electron density curvatures λ_1, λ_2, and λ_3. Bader makes use of an exponential relation which depends on $\rho(\mathbf{r}_{BCP})$ only [Eq. (1)].

$$n_{Bader} = \exp[c_1(\rho(\mathbf{r}_{BCP}) - c_2)] \qquad (1)$$

The parameters c_1 and c_2 can be derived from theoretical calculation on model compounds.

A relationship that also uses the λ_i is given by Equation (2),[8] in which the coefficients a to d, from molecular theoretical calculations, are reported for a number of bond types in the literature.[8,9]

$$n_{top} = a + b \cdot \lambda_3 + c(\lambda_1 + \lambda_2) + d\rho(\mathbf{r}_{BCP}) \qquad (2)$$

For C−C bonds ($a = -0.522$, $b = -1.695$, $d = 8.473$) the coefficient c is equal to zero, so that for this bond n_{top} no longer depends on the perpendicular curvatures λ_1 and λ_2.

In Figure 5 we have plotted the bond orders described above for the different C−C bond types found in $C_{60}Cl_{30}$; for completeness also the Pauling bond order n_p[10] [Eq. (3)], which uses the bond length only, is shown.

$$n_p = \exp[(1.521 - d)/0.293] \qquad d = \text{C−C distance} \qquad (3)$$

While otherwise the agreement between the different types of bond orders is reasonable, the experimental n_{top} values are too small. The reason is the contribution of λ_3 to the n_{top} expression. It is generally known that among the experimental bond topological indices the parallel curvature, λ_3, is the least reproducible[1,11,12] and tends to be considerably larger than the corresponding value from theory. It follows that with the present theoretically derived parameterization of the n_{top} expression experimental bond orders become too small.

In the following discussion all mentioned bond orders (from experiment and theory) were obtained from Bader's exponential relation (the parameters $c_1 = 1.02289$, $c_2 = 1.64585$ were used, derived from an earlier theoretical calculation[13]). For the C_{60} cages of both compounds we find a bond order range from double bond to values significantly smaller than a single bond for both of the halogenated derivatives.

In the diagram for $C_{60}Cl_{30}$ (Figure 3) two rather broad data-point clusters can be recognized. The first one is in the bond length range 1.35–1.40 Å, which belongs to the aromatic bonds of the planar ring system (a′, a″) and the trannulene belt (i, h; see Schlegel diagram) with bond orders between $n = 1.5$ and $n = 2$. The distribution in this cluster corresponds to a C−C bond length range which includes the precise value that is found for the 6/6 bond in free C_{60}. The second cluster is in the bond length range close to 1.5 Å, including sp²–sp³ bond types b, f, g. Bond orders are between $n = 1$ and $n = 1.5$ and one of the carbon atoms involved in the bond is also bound to a Cl atom. No bond appears at the length found for the 5/6 bond in free C_{60}.

Three further small clusters, around bond lengths close to 1.58, 1.63, and 1.69 Å are for bonds of c, d, and e type. They all refer to unusually long sp³–sp³ C−C bonds and hence bond orders smaller than $n = 1$ are derived. They have in common that both carbon atoms involved in forming these three types of bonds are also bound to a Cl atom.

The clustering for $C_{60}F_{18}$ (Figure 4) is as follows: One broad range for bond lengths at 1.35–1.40 Å exists including the aromatic bonds a′ and a″, and the 6/6 bonds of type i, l, n, q in the nondistorted part of the molecule. Consequently the 5/6 bonds j, k, m, o, p, r in the nondistorted region cluster around the bond length range 1.42–1.47 Å, so that the bonding situation in this hemispherical region is not far from that of free C_{60}: Bond orders between $n = 1.5$ and $n = 2$
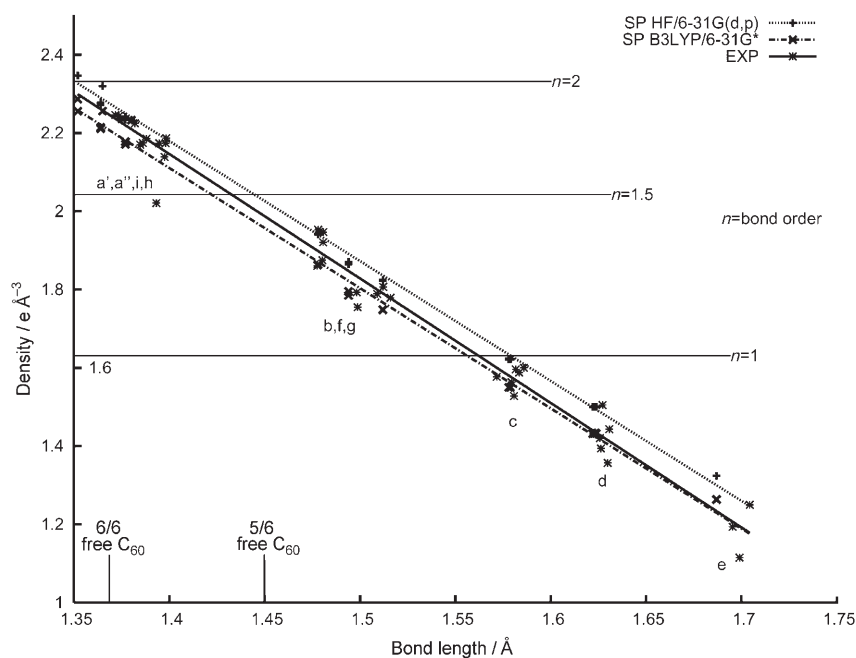
Figure 3. Plot of $\rho(\mathbf{r}_{BCP})$ values [$e\,Å^{-3}$] versus bond lengths [Å] for the C—C bonds in $C_{60}Cl_{30}$ by using results from experiment and the two theoretical calculations. Small letters refer to the bond types given in Figure 2 (bottom).

Figure 4. Plot of $\rho(\mathbf{r}_{BCP})$ values [$e\,Å^{-3}$] versus bond lengths [Å] for the C—C bonds in $C_{60}F_{18}$ by using results from experiment and the two theoretical calculations. Small letters refer to the bond types given in Figure 1 (bottom).

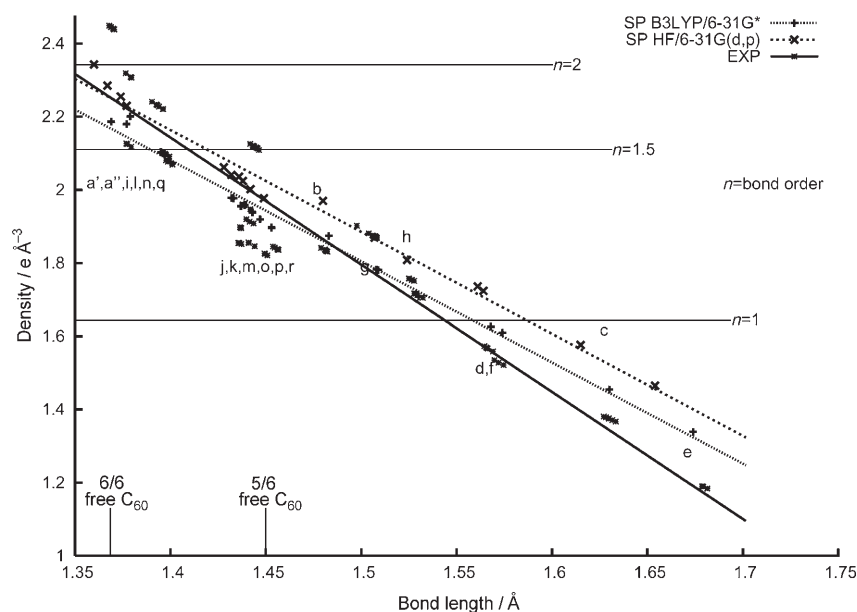can be assigned to the bonds of the first cluster, while the second cluster refers to bond orders $n = 1.3–1.5$. No further distinct clustering is seen. The 5/6 bonds of type b, g, h, for which one of the contributing carbon atoms carries a fluorine atom, have bond orders somewhat above $n = 1$. The longest bonds with bond orders clearly below $n = 1$ belong to

5/6 bonds (type c and e) in which both contributing carbon atoms are also bound to a fluorine atom.

It is known that the elongated C—C bonds of $C_{60}Cl_{30}$ and $C_{60}F_{18}$ can be attacked by oxygen, resulting in their cleavage and formation of intermolecular ethers.[7,14–16] In case of $C_{60}Cl_{30}$, bonds like C10—C11 (bond type e, see Schlegel diagram Figure 2, bottom) show a bent character despite the extreme bond length. Figure 6 shows the Laplacian distribution of the five-membered ring containing the C10—C11 bond. It can be seen that the minimum of the saddle shape of this bond is not localized on the internuclear vector between the two atoms. A similar C—C bond was found in a barbaralane derivative,[13] in which one bond of a three-membered ring was found to have a bond length of 1.65 Å and a $\rho(\mathbf{r}_{BCP}) = 1.29\,e\,Å^{-3}/\bigtriangledown^2\rho(\mathbf{r}_{BCP}) = -1.3\,e\,Å^{-5}$. In both cases the distance between the internuclear vector and the BCP is 0.06 Å (while for a bond in a cyclopropane ring a distance of 0.08 Å is observed).

Atomic properties: Following Bader's AIM theory[3] a molecule can be partitioned into submolecular fragments. The partitioning procedure to obtain atomic regions makes use of the zero-flux surfaces in the electron density gradient vector field $\bigtriangledown\rho(\mathbf{r})$. In order to evaluate the atomic volumes and charges, the algorithm available through the TOPXD program[17] was applied. Averaged results for the various atom types are summarized in Tables 2 and 3 (tables containing atomic properties of each atom are in the Supporting Information). The total atomic volumes (V_{tot}) are defined by the interatomic boundaries in the crystal. It is common practice to consider also the V_{001} volumes, defined by a cutoff at $\rho = 0.001$ au; these volumes are used to compare with charge densities of isolated molecules. Bader
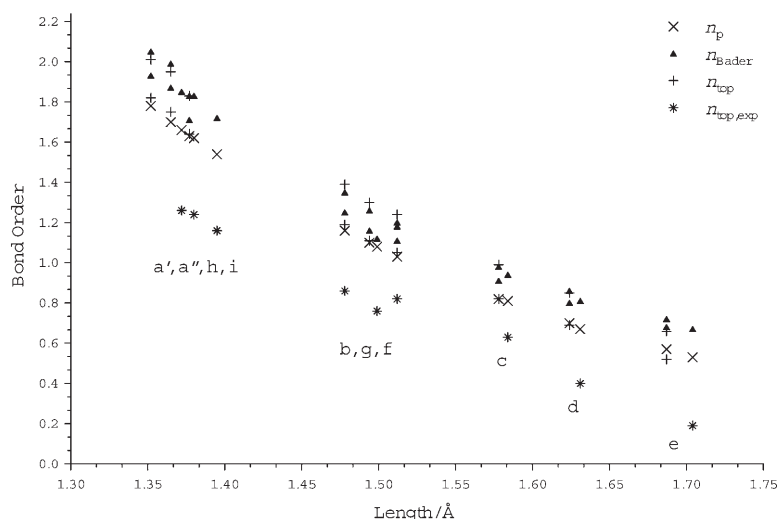
Figure 5. Bond orders, calculated according to the various definitions given in the text, plotted versus the lengths of the different C−C bond types of $C_{60}Cl_{30}$. Small letters indicate the bond types given in the Schlegel diagram, see Figure 2 (bottom).

the unit cell volume within less than 1% , whereas the charges add up to zero. For $C_{60}Cl_{30}$ the sum of charges is also very close to zero (0.02 e), whereas a difference between the sum of V_{tot} and the experimental cell volume of 4.6% is caused by the presence of the additional partially occupied Cl site[7] that was not included in the integration.

It follows from the definition and the data listed in Tables 2 and 3 that V_{tot} is larger than V_{001}. For the carbon atoms the average $\Delta V = V_{tot} - V_{001}$ is 0.58 Å^3 in $C_{60}Cl_{30}$ and 0.93 Å^3 for the fluorine derivative. For the halogen atoms, which are at
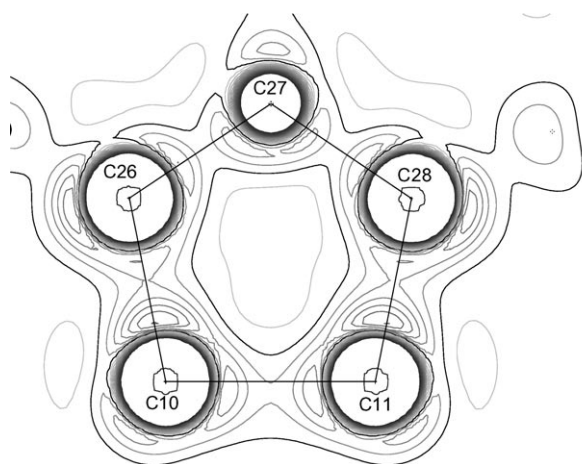

Figure 6. Laplace distribution in one of the five-membered rings of $C_{60}Cl_{30}$ containing the long C−C bond C10–C11 = 1.6886(4) Å. Contour interval 5 e Å^{-5}, black = zero line, gray = negative values, continuous regions next to nuclei = positive.

Table 2. Averaged atomic properties (in Å^3 and e) for the different atom groups in $C_{60}Cl_{30}$.

Group	Type	N[a]	V_{tot}	V_{001}	Q	Cl_{add}
A	C	6	9.11(9)	8.47(9)	0.07(1)	no
B	C	6	6.48(4)	6.43(3)	0.06(1)	yes
C	C	6	6.47(3)	6.43(2)	0.10(1)	yes
D	C	3	6.02(5)	6.00(5)	0.18(1)	yes
E	C	3	9.86(4)	9.02(3)	−0.05(1)	no
F	C	6	9.8(2)	9.0(1)	−0.09(2)	no
G	Cl	6	28.4(15)	26.2(7)	−0.13(1)	
H	Cl	3	28.5(10)	25.4(2)	0.06(1)	
I	Cl	6	30.5(12)	26.3(3)	−0.08(1)	

[a] N = number of contributing atoms.

Table 3. Averaged atomic properties (in Å^3 and e) for the different atom groups in $C_{60}F_{18}$.

Group	Type	N[a]	V_{tot}	V_{001}	Q	F_{add}	$F_{neighbor}$[b]
A	C	6	9.7(3)	9.1(1)	−0.05(1)	no	1
B	C	6	5.67(2)	5.66(2)	0.50(1)	yes	2
C	C	3	5.34(3)	5.34(3)	0.80(1)	yes	3
D	C	6	5.62(2)	5.61(2)	0.68(1)	yes	2
E	C	3	6.22(1)	6.20(1)	0.49(1)	yes	1
F	C	6	10.5(7)	9.6(2)	−0.06(1)	no	1
G	C	6	10.3(10)	9.1(2)	0.05(1)	no	1
H	C	3	11.0(2)	9.5(1)	0.15(1)	no	0
I	C	3	13.0(13)	10.6(3)	−0.25(1)	no	0
J	C	6	11.0(15)	9.6(3)	−0.03(1)	no	0
K	C	6	11.0(16)	9.4(3)	0.15(1)	no	0
L	C	6	11.6(14)	10.1(3)	0.21(1)	no	0
M	F	6	18.4(17)	14.7(4)	−0.63(1)		
N	F	3	16.2(12)	14.0(3)	−0.73(1)		
O	F	6	20.0(26)	15.1(4)	−0.65(1)		
P	F	3	19.8(23)	15.7(2)	−0.83(1)		

[a] N = number of contributing atoms. [b] $F_{neighbor}$ gives the number of fluorinated neighboring carbon atoms.

atomic volumes and charges are additive. The sum of atomic volumes in a given unit cell should be equal to the experimental cell volume. Similarly the sum of all atomic charges should add up to zero. For $C_{60}F_{18}$ the sum of V_{tot} reproduces

peripheral sites of the fullerenes, this difference is larger, that is, $\Delta V = 3.20$ and 3.93 Å^3 for the Cl and F derivatives, respectively. Since the outer regions of the atomic electron density do not contribute significantly to the charge integration, the Q_{tot} and Q_{001} values are practically equal, so that only one Q quantity is given in Tables 2 and 3.

In line with their chemical environments the carbon atoms of $C_{60}Cl_{30}$ can be grouped into six types (see Schlegel diagram and Table 2). The aromatic carbon atoms of group E and F of the trannulene belt (C22–C30) are the largest ones (average $V_{tot}/V_{001} = 9.86(4)/9.02(3)$ Å^3 for E, and 9.8(2)/ 9.0(1) Å^3 for group F, quantities in parentheses are the standard deviations with respect to the sample means), while the aromatic carbons of the planar six-membered ring (C1– C6) belonging to group A have a slightly reduced volume

($V_{tot}/V_{001} = 9.11(9)/8.47(9)$ Å^3). The sp^3 carbon atoms of group B, C, and D (C7–C21), each carrying a chlorine atom, have a strongly reduced volume of $V_{tot}/V_{001} = 6.48(4)/6.43(3)$ Å^3 for group B, and $6.47(3)/6.43(2)$ Å^3 and $6.02(5)/6.00(5)$ Å^3 for groups C and D, respectively. Evidently for the last two types of atoms the crystal environment does not influence the atomic volume so that V_{tot} and V_{001} are practically equal. For all chlorine atoms (groups G–I) an averaged volume of $V_{tot}/V_{001} = 29.3(17)/26.1(6)$ Å^3 is observed.

From the experimentally obtained atomic charges all atoms can be regarded as almost neutral. The benzenoid carbon atoms and the sp^3 carbon atoms are slightly positively charged (0.07/0.10 e), which is compensated by small negative charges of the carbons of the trannulene belt (−0.08 e).

The integration of the atomic basins in $C_{60}F_{18}$ led to a wide range of volumes and charges for the carbon atoms, and a more narrow range for the corresponding properties of fluorine atoms. Although the space group does not provide crystallographic 3mm symmetry for the molecule, a grouping of the atoms according to this symmetry can be applied. We consider 12 groups for the carbon atoms and four fluorine atom groups (see Schlegel diagram and Table 3) that can be distinguished with respect to their volumes or charges. While the atoms C1–C6 belonging to group A and the atoms of groups F–L are not fluorine-substituted, atoms of group B–D carry a fluorine atom. For the following discussion we also consider for each carbon atom whether or not its neighboring carbon atoms are fluorinated.

Members of group C, which are all bound to fluorine atoms and, in addition, all of their three carbon neighbors are also bound to fluorine atoms, have the smallest volume of $V_{tot}/V_{001} = 5.34(3)/5.34(3)$ Å^3 and the highest positive charge of 0.8 e. Groups B and D contain carbon atoms bound to fluorine and with two fluorine-bound neighboring carbon atoms. They have a slightly larger volume of $5.64(3)/5.64(3)$ Å^3 (averaged over B and D) and a smaller positive charge of 0.50(1) e for B and 0.68(1) e for D. The last group of carbon atoms bound to fluorine are in group E. Only one of their three carbon neighbors is also bound to fluorine and we find a volume of $6.22(1)/6.20(1)$ Å^3 and a charge of 0.49(1) e. For the non-fluorine-bound carbon atoms in groups A, F, and G one neighboring carbon atom is always fluorinated. The atoms in the planar aromatic ring (group A) occupy basins with a volume of $9.7(3)/9.1(1)$ Å^3, while the F and G volumes are very similar [$10.5(7)/9.6(2)$ Å^3 for F and $10.3(10)/9.1(2)$ Å^3 for G]. All charges of A, F, and G group atoms are very close to zero. For the other carbon atom groups H to L (no fluorine-bound neighboring carbon atom), no general trend for the volumes and charges can be seen, except that the volumes tend to have larger values than for the groups considered before. It should also be noted that for the fluorine-bound carbon atoms the V_{tot} and V_{001} volumes are practically equal, so that the average difference between the two types of volumes is caused only by the non-fluorine substituted carbon atoms. This holds also for the $C_{60}Cl_{30}$ case.

The fluorine atoms (groups M–P) have volumes of, roughly, 16–20 Å^3 for V_{tot} and 14–16 Å^3 for V_{001}, and no significant differences for the four groups are seen. They all have strong negative charges between −0.63 e and −0.83 e. Fluorine is known to have very constant atomic volumes and charges independent of the hybridization status of the carbon atom it is bound to.[18] In previous studies on fluoro-substituted hydrocarbons[19,20] fluorine volumes and charges in the same range as found in this study were reported.

For free C_{60} a V_{001} volume of 11.0 Å^3 was derived (see Table 1). Although an experimental charge density study of free C_{60} does not exist, a V_{tot} can be estimated from the molecular volume (694 Å^3) obtained from the cell volume of the crystal structure.[21] From the $V_{tot} = 11.6$ Å^3 thus obtained and taking $V_{001} = 11.0$ Å^3 from Table 1, it follows that all the carbon atoms of $C_{60}Cl_{30}$ and most of the carbon atoms of $C_{60}F_{18}$ are significantly smaller than in free C_{60}. Only a few atoms in the almost nondistorted region opposite to the fluoro-substituted side approach the free C_{60} atomic volume. Consequently the total volume of the C_{60} cage in the halogenated compounds is considerably reduced compared to free C_{60} being 76/80 % (based on V_{001}/V_{tot}) of the F and even 69 % of the Cl compound. It follows that the halogen addition does not only lead to a dramatic distortion of the C_{60} cage, but also to a significant reduction of its volume.

Hirshfeld surfaces: Figure 7 depicts Hirshfeld surface[22,23] representations of $C_{60}F_{18}$. It can be seen on the color-gradient legend that the crystal electron density mapped on the surface varies from zero to 0.075 e Å^{-3}. This is a very small value compared to other interactions like hydrogen bonds for which this quantity can reach values around 0.25 e Å^{-3}. So it can be concluded that in $C_{60}F_{18}$ intermolecular contacts are very weak, if even present. The strongest local density can be seen around C54 on Figure 7 (top) or around F12 on Figure 7 (bottom), which is a kind of sheer plan of the surface to visualize the interior of the surface. This density of 0.075 e Å^{-3} belongs to the intermolecular contact C54···F12 of 2.8 Å, which is not the shortest contact the molecules have in this structure. The shortest contact is between F2 and F14 with a distance of 2.75 Å and a density of only 0.05 e Å^{-3}. It is interesting to note that in all C···F contacts, the surface is concave at the carbon site and convex at the fluorine site. The smaller polarizability of the fluorine atoms may be the reason for this behavior.

Electrostatic potential: Figure 8 depicts representations of the electrostatic potentials of both molecules mapped on the iso-surface of the electron density at a value of 0.5 e Å^{-3}. The visualization was created with MOLISO,[24] a program which was written by one of the authors. The electronegativity difference between carbon and fluorine and the addition to one hemisphere of the fullerene cage leads to a strong potential gradient along the $C_{60}F_{18}$ molecule.

In case of the $C_{60}Cl_{30}$ molecule the differences are not so pronounced as for $C_{60}F_{18}$. This makes sense in that the elec-
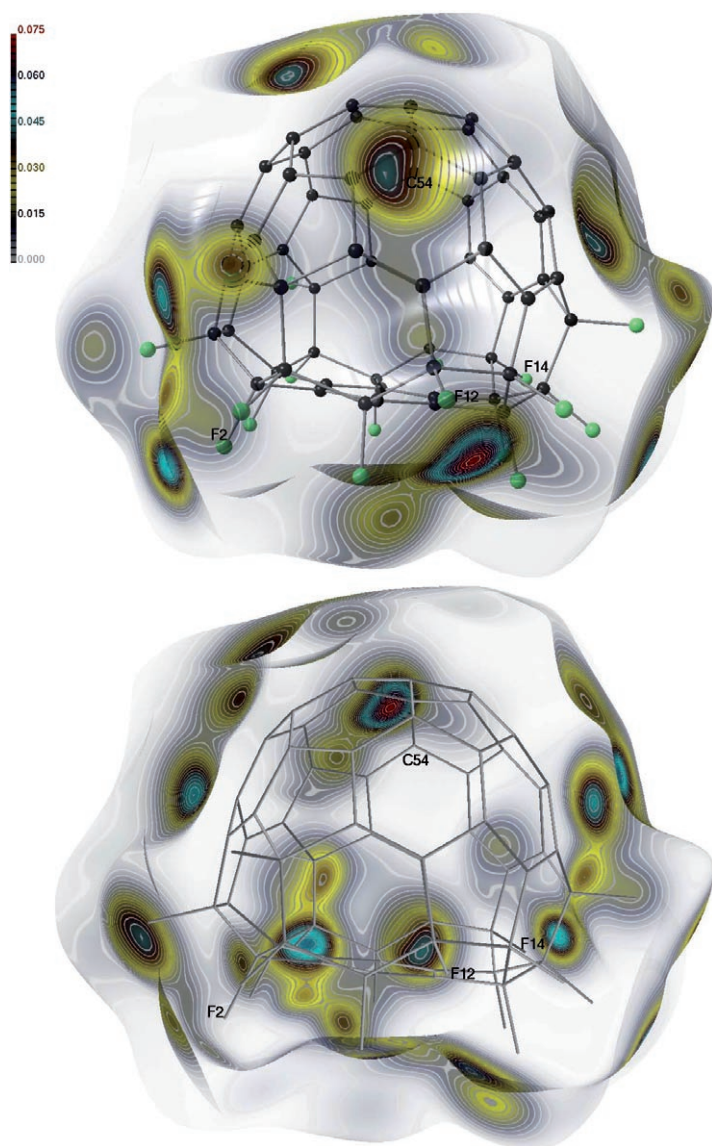
Figure 7. Hirshfeld surface of $C_{60}F_{18}$. Top: front side of the surface; bottom: sheer plan representation. The color code (see color bar) gives the value of the crystal electron density on the surface. Drawing generated with MOLISO.[24]

tronegativity difference between Cl and C is much smaller than between F and C.

Conclusion

As already stated in the introduction fullerene crystals generally suffer from several shortcomings that rarely allow accurate high-resolution X-ray data to be collected for charge density work. In this respect the title compounds represent two extreme examples. On the one hand $C_{60}Cl_{30}$ is an exception in that crystals of sufficient size and quality could be grown so that primary radiation from a conventionally sealed Mo X-ray tube was sufficient to collect a suitable data set. In addition the ultra low temperature of 20 K sup-

ported the measurement of significant high-order reflections. On the other hand $C_{60}F_{18}$ is an example for which it was hopeless, from the point of view of the crystal size and diffraction properties, to measure an appropriate data set under home laboratory conditions. Only the highly brilliant primary intensity of a focused beam at the synchrotron beamline X10SA of the SLS[25] allowed the collection of a data set with considerable amount of significant reflections also in the high-order region, so that these particular experimental conditions provided the unique chance for a charge density study of $C_{60}F_{18}$.

Due to halogen addition, the two fullerene cages have C−C bonds of very different lengths and several distinguishable carbon atoms. For the C−C bonds the BCP properties were compared to each other and to those derived by theoretical methods at HF/6−31G(d,p) and B3LYP/6−31G* levels. While for the Cl compound the experimental values are intermediate between the two theoretical data sets, the spread between experiment and theory is more pronounced for the F derivative, which can be attributed to the limited crystal quality that resulted in a somewhat reduced-quality data set. Bond orders that were derived from the $\rho(\mathbf{r}_{BCP})$'s cover a range from $n=2$ to values considerably below $n=1$ for 5/6 bonds for which halogen atoms are bound to both contributing carbon atoms.

The carbon atomic volumes were all found to be smaller than those in free C_{60}, with the individual volumes depending on whether or not they carry a halogen atom. In case of the fluorine compound, even the influence of a fluorine atom on the next nearest neighbor was seen. In total the halogen addition not only leads to an unusual shape of the C_{60} cage, but also to a significant reduction of its volume compared to the highly symmetrical free C_{60} sphere.

Together with our earlier study,[1] electron densities were examined on highly substituted (almost) nondistorted and distorted C_{60} cages with multiple additions. Corresponding studies on a weakly or nonsubstituted C_{60} sphere with a small number of addends would be desirable. The same holds for a C_{70} fullerene, for which until now—as far as we know—no experimental charge density determination is known, but is in progress in our group.

Experimental Section

CCDC–626375 and CCDC-626376 contain the supplementary crystallographic data for this paper. These data can be obtained free of charge from The Cambridge Crystallographic Data Centre via www.ccdc.cam.ac.uk/data_request/cif.

X-ray diffraction experiments: $C_{60}Cl_{30}$ in the form of well-shaped crystals was prepared by ampoule reaction between C_{60} and $SbCl_5$ at 280–300 °C.[14] $C_{60}F_{18}$ was prepared in a 4 h reaction between C_{60} and K_2PtF_6 in an approximate 1:4 molar ratio at 460–465 °C. Subsequent purification by fractional sublimation[5] yielded a $C_{60}F_{18}$ sample, the purity of which was sufficient for growing brown needle-shaped single crystals of this compound by sublimation in the evacuated ampoule in the temperature gradient 450→380 °C.

$C_{60}Cl_{30}$ is one of the rare cases of a fullerene derivative that gives nicely diffracting crystals of sufficient size so that primary X-radiation from a
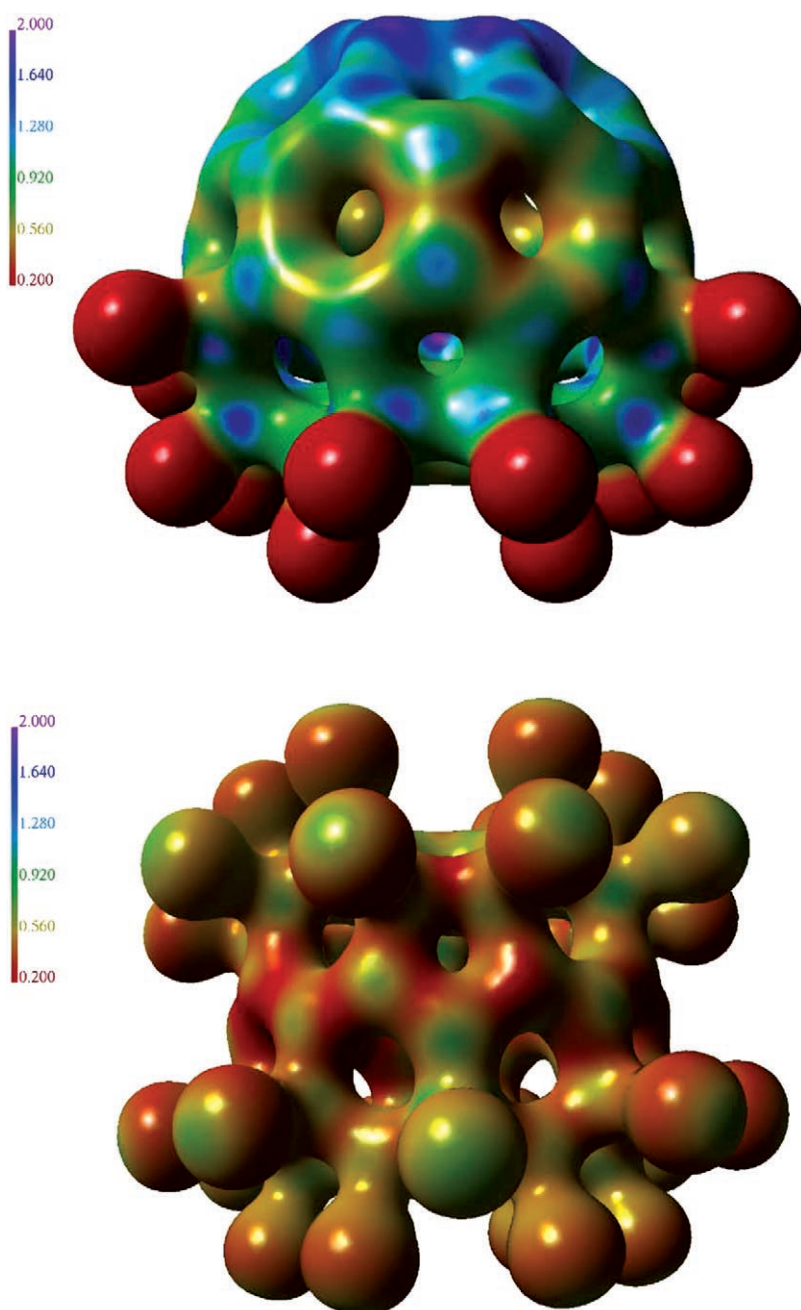
Figure 8. Electrostatic potentials of $C_{60}F_{18}$ (top) and $C_{60}Cl_{30}$ (bottom) calculated from the experimental charge densities and mapped onto the isoelectron density surface $\rho = 0.5$ e Å^{-3}. The color code is shown by the color bar (drawing generated with MOLISO[24]).

In contrast to $C_{60}Cl_{30}$, only extremely thin, needle-shaped crystals of $C_{60}F_{18}$ were available with tiny dimensions in two directions. Diffraction properties were poor even in the low-order region in front of a sealed X-ray tube. The only data collection of acceptable quality could be performed at the protein beam line X10 SA of the Swiss Light Source (SLS) at Paul Scherrer Institute (Villigen, Switzerland), with the brilliant primary intensity of a focused beam (focus size 50×10 μm^2, $H \times V$, fwhm, wavelength $\lambda = 0.6214$ Å) could be used.[25]

The experimental setup of this beam-line, which is normally designed for protein crystallography, was—for the first time for our experiment—modified to allow the collection of high-resolution data from our crystal. For that purpose a movement of the MAR225 CCD area detector was adjusted to allow variable 2θ detector positions. An arc (4DX-ray System AB) mounted on the goniometer head allowed us to simulate different χ-positions so that the limitations from the otherwise single-axis geometry of the diffractometer could be reduced. With this setup 245 274 reflections could be measured at $T = 92$ K in a beam-time period of approximately 2 h. Data were processed with XDS[29] and reduced to give 14 715 unique reflections (Friedel pairs merged, for further details see Table 4). Due to the first use of the mechanically modified diffractometer a few experimental limitations had to be accepted. It was, for example, geometrically not possible to reach outer regions of reciprocal space with $\sin\theta/\lambda > 1.0$ Å^{-1}, although the brilliant primary radiation would have allowed the collection of significant intensity data far beyond this resolution, as the mean I/σ ratio of 41.0 in the highest measured resolution shell showed.[30] It cannot be ruled out that the data set was further affected by the crystal quality. We used the "biggest" crystal we could obtain (dimension $1.0 \times 0.1 \times 0.06$ mm) for the data collection; however, optical inspection showed various impurities like powder particles and small crystalline satellites on the crystal surface that were not removed because of the risk of destroying the crystal. The adhesions were visible as weak powder lines and further contaminations in the diffraction pattern so that in spite of the high intensity output the data set may suffer from the above mentioned shortcomings.

Multipole refinements: The known atomic parameters from conventional spherical atom refinement were taken to establish the starting positional and displacement parameters for the subsequent aspherical atom analysis. This was based on the Hansen–Coppens multipole formalism[31] implemented in the XD program package.[17] In all refinements the quantity $\Sigma_H w_H(|F_o(H)| - k|F_c(H)|)^2$ was minimized by using the statistical weight $w_H = \sigma(F_o(H))^{-2}$ and only those structure factors which met the criterion $F_o(H) > 2.5\sigma(F_o(H))$ were included.

sealed tube was sufficient for a high-resolution data collection. An accurate data set was measured by using $Mo_{K\alpha}$ radiation (graphite monochromator) at 20 K on a large four-circle Eulerian cradle (Huber, type 512) equipped with a double-stage closed cycle He cryostat (Displex, Air Products, USA) and a Bruker- APEX area detector.[26] For the data collection and integration SMART and SAINT routines[26] were used. A total of 248 726 reflections were measured up to a resolution of $\sin\theta/\lambda = 1.168$ Å^{-1} (or $d = 0.43$ Å); these were merged with SORTAV[27] to give 36 787 unique reflections. Due to the rather high absorption coefficient an analytical absorption correction was performed with refined face distances.[28] Further details on the crystal data and the experimental conditions are given in Table 4.

Table 4. Crystallographic and refinement details.

	$C_{60}F_{18}$	$C_{60}Cl_{30}$
formula	$C_{60}F_{18}$	$C_{60}Cl_{30} \times 0.097\ Cl_2$
M_r [g mol^{-1}]	1062.62	1790.98
crystal system	monoclinic	monoclinic
space group	Cc	$P2_1/n$
Z	4	2
T [K]	92	20
a [Å]	19.669(4)	12.520(1)
b [Å]	11.041(1)	13.479(1)
c [Å]	19.160(2)	17.088(2)
β [°]	120.26(1)	99.95(1)
V [Å^3]	3593.8(9)	2840.5(5)
ρ_{calcd} [g cm^{-3}]	1.96	2.094
μ [mm^{-1}]	0.18	1.49
min/max transmission	–/–	0.51/0.57
crystal shape	needle	block
crystal dimensions [mm]	$1.0 \times 0.1 \times 0.06$	$0.45 \times 0.4 \times 0.35$
radiation λ [Å]	0.6214	0.71073
$(\sin\theta/\lambda)_{max}$ [Å^{-1}]	1.00	1.168
collected reflections	245 274	248 726
completeness [%]	98.6	96.4
unique reflections	14 847	36 787
redundancy	16.8	6.6
R_{int}	0.043	0.032
observed reflections [$F_o > 2.5\sigma(F_o)$]	14 715	30 212
R value (spherical)	0.0373	0.0205
multipole refinement:		
N_v	806	598
R_F	0.0289	0.0165
R_{all}	0.0291	0.0252
R_{wF}	0.0336	0.0174
R_{F2}	0.0700	0.0253
R_{allF2}	0.0700	0.0263
R_{wF2}	0.0672	0.0350
Gof	4.5309	0.9139
N_{ref}/N_v	18.5	50.6

For $C_{60}Cl_{30}$ the multipole model was expanded up to the hexadecapole level ($l=4$) for all atoms except for the atom of the enclosed partially occupied chlorine atom (Cl16), for which only monopole level was used. For the C and Cl atoms the individual radial screening parameters (κ and κ') were assigned and refined. As atomic site symmetry, a cylindrical symmetry was applied for the terminal halogen atoms, while no symmetry for the carbon atoms was applied. Chemically equivalent atoms were constrained; for example, the aromatic carbon atoms. In the multipole model used, a scale factor, the atomic positions, and the anisotropic temperature parameters of the C and Cl atoms were refined together with the multipole parameters. The refinement of 30 212 observed reflections yielded agreement factors of $R=1.65\%$ and $R_w=1.74\%$.

The multipole model of $C_{60}F_{18}$ was refined only up to the octopole level ($l=3$). The introduction of hexadecapole parameters was not considered appropriate, because of the limited resolution of the data set. According to the chemical C_{3v} symmetry of the molecule the 78 atoms of $C_{60}F_{18}$ were subdivided into 16 groups A–P (see Schlegel diagram and Table 3). All the atoms within a group were constrained to each other. For the fluorine atoms, cylindrical symmetry was applied. Mirror symmetry was applied to the carbon atoms of groups C, E, H, and I. All other atoms were not constrained by any symmetry. The resulting 806 parameters were refined on 14 715 observed reflections to a final R value of 2.89% and $R_w=3.36\%$ (for further refinement details, see Table 4).

Theoretical calculations: For a comparison with the experimental results, electron densities were also derived theoretically from ab initio calculations at the Hartree–Fock (HF) and density functional (B3LYP) levels of theory by using the Gaussian 98[32] program package. For $C_{60}F_{18}$ geometry optimizations were calculated with the experimental geometry as input by using HF/6–31G(d,p) and B3LYP/6–31G(d) standard basis sets. For $C_{60}Cl_{30}$ single-point ab initio calculations were carried out with the same basis sets. The topology of the electron densities was analyzed with AIMPAC.[33]

[1] A. Wagner, R. Flaig, D. Zobel, B. Dittrich, P. Bombicz, M. Strümpel, P. Luger, T. Koritsanszky, H.-G. Krane, *J. Phys. Chem. A* **2002**, *106*, 6581–6590.

[2] H. Irngartinger, A. Weber, T. Oeser, *Angew. Chem.* **1999**, *111*, 1356–1358; *Angew. Chem. Int. Ed.* **1999**, *38*, 1279–1281.

[3] R. F. W. Bader, *Atoms in Molecules*, Clarendon, Oxford, **1994**.

[4] I. S. Neretin, K. A. Lyssenko, M. Yu. Antipin, Yu. L. Slovokhotov, O. V. Boltalina, P. A. Troshin, A. Yu. Lukonin, L. N. Sidorov, R. Taylor, *Angew. Chem.* **2000**, *112*, 3411–3415; *Angew. Chem. Int. Ed.* **2000**, *39*, 3273–3276.

[5] I. V. Goldt, O. V. Boltalina, L. N. Sidorov, E. Kemnitz, S. I. Troyanov, *Solid State Sci.* **2002**, *4*, 1395–1401.

[6] P. B. Hitchcock, R. Taylor, *Chem. Commun.* **2002**, 2078–2079.

[7] P. A. Troshin, R. N. Lyubovskaya, I. N. Ioffe, N. B. Shustova, E. Kemnitz, S. I. Troyanov, *Angew. Chem.* **2005**, *117*, 238–241; *Angew. Chem. Int. Ed.* **2005**, *42*, 234–237.

[8] S. T. Howard, O. Lamarche, *J. Phys. Org. Chem.* **2003**, *16*, 133–141.

[9] V. G. Tsirelson, A. I. Stash, V. A. Potemkin, A. A. Rykounov, A. D. Shutalev, E. A. Zhurova, V. V. Zhurov, A. A. Pinkerton, G. V. Gurskaya, V. E. Zavodnik, *Acta Crystallogr. Sect. B* **2006**, *62*, 676–688.

[10] L. Pauling, *The Nature of the Chemical Bond*, Cornell University Press, Ithaca, NY, **1960**, p. 144.

[11] R. Bianchi, C. Gatti, V. Adivasio, M. Nardelli, *Acta Crystallogr. Sect. B* **1996**, *52*, 471.

[12] A. Volkov, Y. Abramov, P. Coppens, C. Gatti, *Acta Crystallogr. Sect. A* **2000**, *56*, 332.

[13] P. Luger, M. Messerschmidt, S. Scheins, A. Wagner, *Acta Crystallogr. Sect. A* **2004**, *60*, 390–396.

[14] S. I. Troyanov, N. B. Shustova, A. A. Popov, L. N. Sidorov, *Russ. Chem. Bull.* **2005**, *54*, 1656–1666.

[15] O. V. Boltalina, B. de La Vaissiere, P. W. Fowler, P. B. Hitchcock, J. P. B. Sandall, P. A. Troshin, R. Taylor, *Chem. Commun.* **2000**, 1325–1326.

[16] S. I. Troyanov, O. V. Boltalina, I. V. Kuvytchko, P. A. Troshin, E. Kemnitz, P. B. Hitchcock, R. Taylor, *Fullerenes, Nanotubes, Carbon Nanostruct.* **2002**, *10*, 243–260.

[17] T. Koritsánszky, T. Richter, P. Macci, C. Gatti, S. Howard, P. R. Mallinson, L. Farrugia, Z. W. Su, N. K. Hansen, XD—A Computer Program Package for Multipole Refinement and Analysis of Electron Densities from Diffraction Data, Freie Universität Berlin, Berlin (Germany), **2003**.

[18] D. Lentz, M. Patzschke, A. Bach, St. Scheins, P. Luger, *Org. Biomol. Chem.* **2003**, *1*, 409–414.

[19] A. Bach, D. Lentz, P. Luger, *J. Phys. Chem. A* **2001**, *105*, 7405–7412.

[20] A. Bach, D. Lentz, P. Luger, M. Messerschmidt, Ch. Olesch, M. Patzschke, *Angew. Chem.* **2002**, *114*, 311–314; *Angew. Chem. Int. Ed.* **2002**, *41*, 296–299.

[21] S. Liu, Y.-J. Lu, M. M. Kappes, *Science* **1991**, *254*, 408.

[22] J. J. McKinnon, A. S. Mitchell, M. A. Spackman, *Chem. Eur. J.* **1998**, *4*, 2136–2141.

[23] M. A. Spackman, P. G. Byrom, *Chem. Phys. Lett.* **1997**, *267*, 215–220.

[24] C. B. Hübschle, Moliso—A Program for Color Mapped Iso-surfaces Freie Universität Berlin, Berlin (Germany), **2006**.

[25] E. Pohl, C. Pradervand, R. Schneider, T. Tomizaki, A. Pauluhn, Q. Chen, G. Ingold, E. Zimoch, C. Schulze-Briese, *Synchrotron Radiat. News* **2006**, *19*, 24–26.

[26] BRUKER-AXS INC. ASTRO (**1995–1996**), SMART (**1996**), SAINT (**1994–1996**), Madison, WI (USA).

[27] R. H. Blessing, *J. Appl. Crystallogr.* **1997**, *30*, 421.

[28] M. Lutz, Euhedral Tutorial, Utrech University **2003**.

[29] W. Kabsch, *J. Appl. Crystallogr.* **1993**, *26*, 795–800.

[30] P. Luger, A. Wagner, Ch. B. Hübschle, S. I. Troyanov, *J. Phys. Chem. A* **2005**, *109*, 10177–10179.

[31] N. K. Hansen, P. Coppens, *Acta Crystallogr. Sect. A* **1978**, *34*, 909.

[32] Gaussian 98, Revision A.7, M. J. Frisch, G. W. Trucks, H. B. Schlegel, G. E. Scuseria, M. A. Robb, J. R. Cheeseman, V. G. Zakrzewski, J. A. Montgomery, Jr., R. E. Stratmann, J. C. Burant, S. Dapprich, J. M. Millam, A. D. Daniels, K. N. Kudin, M. C. Strain, O. Farkas, J. Tomasi, V. Barone, M. Cossi, R. Cammi, B. Mennucci, C. Pomelli, C. Adamo, S. Clifford, J. Ochterski, G. A. Petersson, P. Y. Ayala, Q. Cui, K. Morokuma, D. K. Malick, A. D. Rabuck, K. Raghavachari, J. B. Foresman, J. Cioslowski, J. V. Ortiz, A. G. Baboul, B. B. Stefanov, G. Liu, A. Liashenko, P. Piskorz, I. Komaromi, R. Gomperts, R. L. Martin, D. J. Fox, T. Keith, M. A. Al-Laham, C. Y. Peng, A. Nanayakkara, C. Gonzalez, M. Challacombe, P. M. W. Gill, B. Johnson, W. Chen, M. W. Wong, J. L. Andres, M. Head-Gordon, E. S. Replogle, , J. A. Pople, Gaussian, Inc., Pittsburgh PA, **1998**.

[33] J. Cheeseman, T. A. Keith, R. W. F. Bader. AIMPAC programm package, McMaster University, Hamilton, Ontario (Canada), **1992**.

[34] M. N. Burnett, C. K. Johnson. ORTEP-III, oak ridge thermal ellipsoid plot program for crystal structure illustrations. Oak Ridge National Laboratory Report ORNL-6895, Oak Ridge, Tennessee, **1996**.